Original Research

Science of Traditional Chinese Medicine

OPEN

Influenza A virus infection activates TLR3-mediated necroptosis

Weijie Li[a], Congying Huang[a], Ziling Zeng[a], Xiang Li[a], Jia Xu[b], Tian Gong[a,c], Hao Zhang[b], Xinyan Zhang[d], Ping Wang[a], Yuanjia Hu[e], Haiyu Xu[a,f,*], Lijuan Song[a,*]

[a]State Key Laboratory for Quality Ensurance and Sustainable Use of Dao-di Herbs, Institute of Chinese Materia Medica, China Academy of Chinese Medical Sciences, Beijing, China; [b]Guang'anmen Hospital, China Academy of Chinese Medical Sciences, Beijing, China; [c]School of Traditional Chinese Materia Medica, Shenyang Pharmaceutical University, Shenyang, China; [d]National Institutes for Food and Drug Control, Beijing, China; [e]State Key Laboratory of Mechanism and Quality of Chinese Medicine, Institute of Chinese Medical Sciences, University of Macau, Macao SAR, China; and [f]Liaoning University of Traditional Chinese Medicine, Dalian, China

Abstract

Background: Influenza A virus (IAV) is a negative-sense RNA virus of the Orthomyxoviridae family and is the etiological agent of a highly contagious acute respiratory disease that can lead to acute lung injury.

Objective: To elucidate the molecular mechanisms of IAV infection, an integrative research approach combining gene expression profiling, multinetwork analysis, and *in vivo* experimental validations was employed.

Methods: First, a series of network-based analyses were performed, including protein–protein interaction network construction, weighted gene co-expression network analysis, and subsequent gene set enrichment analysis, to identify the major underlying mechanisms of IAV infection. Following gene expression analysis, core targets, both direct and indirect regulators, were screened. An IAV (H1N1) strain A/PR/8/34-induced acute lung injury mouse model was constructed for *in vivo* validations. Batch one included two groups to evaluate findings from the multi-network analysis: Mock (n = 10; 5 males and 5 females) and IAV (n = 10; 5 males and 5 females). Batch two included three groups to assess the role of toll-like receptor 3 (TLR3) in IAV infection: Mock (n = 6; 3 males and 3 females), IAV (n = 6; 3 males and 3 females), and TLR3 inhibitor (n = 6; 3 males and 3 females). Body weight was measured on days 0, 3, and 5 after infection. On day 5, lung tissues were collected to assess viral load and histopathological changes. Key targets were examined using enzyme-linked immunosorbent assay, Western blotting, and immunofluorescence staining, both in sera and lung tissues.

Results: IAV infection was significantly associated with dysregulation of the immune-inflammation system, such as the LTR, nucleotide-binding oligomerization domain-(NOD) like receptor, retinoic acid-inducible gene I-like receptor, and nuclear factor kappa-B signaling pathways. Gene set enrichment analysis further indicated that the TLR and necroptosis signaling pathways played crucial roles in the progression of IAV infection (TLR signaling pathway normalized enrichment score = 2.3941, $P = 1.00 \times 10^{-10}$; necroptosis normalized enrichment score = 1.9421, $P = 6.21 \times 10^{-7}$). Among the core targets, TLR3 and mixed lineage kinase domain-like protein (MLKL) may regulate gene expression at the transcriptional level (all $P < 0.05$). *In vivo* validation using an IAV (PR8) infected acute lung injury mouse model demonstrated increased viral load and lung index, alveolar structural damage, and inflammatory cell infiltration. Immunofluorescence staining exhibited large gaps in Lamin B1 staining and breaches in Emerin signals following IAV-PR8 infection. Expression levels of TLR3, p-receptor-interacting serine/threonine-protein kinase 3 (RIPK3)/RIPK3, and p-mixed lineage kinase domain-like protein (MLKL)/MLKL proteins in lung tissues, as well as proinflammatory factors and mediators in sera, were significantly elevated after IAV infection. Moreover, enhanced neutrophil infiltration (myeloperoxidase) and citrullinated histone H3 (a neutrophil extracellular trap–specific marker), both established indicators of neutrophil extracellular trap formation, were observed. Notably, treatment with a TLR3 inhibitor significantly ameliorated IAV-induced acute lung injury by regulating necroptosis-related targets.

Conclusion: Our study provides network-based *in vivo* evidence that TLR3-receptor-interacting serine/threonine-protein kinase 3-MLKL-mediated necroptosis may underlie IAV-induced acute lung injury and could serve as a potential therapeutic target in severe influenza cases.

Key words: Influenza A virus; Necroptosis; "Immune-inflammation" regulation; TLR3-RIPK3-MLKL signaling; Network analyses

**Corresponding Author: Haiyu Xu, State Key Laboratory for Quality Ensurance and Sustainable Use of Dao-di Herbs, Institute of Chinese Materia Medica, China Academy of Chinese Medical Sciences, No. 16, Nanxiaojie, Dongzhimennei, Beijing 100700, China. E-mail address: hyxu@icmm.ac.cn (H. Xu). Lijuan Song, State Key Laboratory for Quality Ensurance and Sustainable Use of Dao-di Herbs, Institute of Chinese Materia Medica, China Academy of Chinese Medical Sciences, No. 16, Nanxiaojie, Dongzhimennei, Beijing 100700, China. E-mail address: ljsong@icmm.ac.cn (L. Song).*

Science of Traditional Chinese Medicine, (2026) 4, 1, 40–49

Supplemental digital content is available for this article. Direct URL citations are provided in the HTML and PDF versions of this article on the journal's Web site (www.stcm.com).

Received July 21, 2025; Accepted September 09, 2025

http://dx.doi.org/10.1097/st9.0000000000000093

1. Introduction

Seasonal human influenza viruses cause acute respiratory infections that affect the entire population, resulting in approximately 650,000 deaths annually worldwide and imposing a significant public health and economic burden.[1] Influenza A virus (IAV), a negative-sense RNA virus of the Orthomyxoviridae family, is the etiological agent of this highly contagious acute respiratory disease.[2,3] Influenza outbreaks lead to substantial morbidity and mortality each year, particularly from pneumonia in the elderly.[4–6] Vaccination is currently considered the most effective strategy for preventing or mitigating the disease caused by co-circulating influenza A and B viruses.[7] However, seasonal influenza vaccines primarily utilize inactivated viruses, and the virus's ability to evade host antiviral immune responses necessitates annual strain updates.[8] Therefore, elucidating the pathogenic mechanisms of IAV infection is essential for the development of more effective vaccines and novel antiviral therapies.

Recent studies have indicated that IAV activates multiple programmed cell death pathways, including apoptosis, necrosis, necroptosis, and pyroptosis, which play essential roles in host defense against viral infection and replication.[9] The elimination of infected cells through programmed cell death is a well-established mechanism for limiting viral spread. Among these pathways, necroptosis is a form of caspase-independent necrotic cell death triggered by bacterial and viral infections and is mainly regulated by receptor-interacting serine/threonine-protein kinase 3 (RIPK3), receptor-interacting serine/threonine-protein kinase 1 (RIPK1), and mixed lineage kinase domain-like protein (MLKL).[10,11] Both RIPK1 and RIPK3 contain an N-terminal kinase domain followed by a RIP homotypic interaction motif.[12] Physical interactions among RIPK1, RIPK3, and MLKL within the necrosome complex induce MLKL phosphorylation, leading to its oligomerization and execution of necroptotic cell death.[13,14]

Clinical practice has demonstrated that traditional Chinese medicine (TCM) holds unique advantages in treating influenza virus infection, as it exerts both direct antiviral effects and modulates immune-inflammatory imbalances. Elucidating the key molecular mechanisms underlying the progression of viral infection is crucial for developing precise therapeutic strategies. This study aims to advance the mechanistic research on TCM against the influenza virus and to provide actionable drug targets for screening natural products. However, the critical role of necroptosis in influenza pathogenesis, as well as the underlying mechanisms of IAV-mediated necroptosis, remains unclear. In this study, high-quality transcriptome data were used to construct protein–protein interaction (PPI) network and perform enrichment analyses to identify hub genes. Furthermore, weighted gene co-expression network analysis and gene set enrichment analysis (GSEA) were applied to uncover potential key regulatory targets involved in disease pathogenesis. Experimental validation was then conducted using an IAV-PR8-induced acute lung injury mouse model. Collectively, our study provides new insights into the pathogenesis of IAV infection and may facilitate the development of natural product screening.

2. Materials and methods

2.1. Data mining and analysis

Transcriptome data were downloaded from the Gene Expression Omnibus (GEO) database (GEO accession No. GSE163959).[15] The dataset comprises lung tissues from 5 individuals that were either IAV- or mock-infected and subsequently analyzed for transcriptome profiling, with a focus on innate immune responses. IAV-related genes, defined as differentially expressed genes (DEGs) between the IAV-infected and mock-infected groups, were identified using the criteria of t test $P < 0.05$ and |fold change| > 1.

2.2. Network construction and analysis

The IAV-related gene interaction network was constructed and analyzed based on the interactions among DEGs between the IAV-infected and mock-infected groups to identify key IAV-related genes. First, PPIs were established using the search tool for recurring instances of neighbouring genes (STRING) database (version 12.0, http://string-db.org/), with a combined score >0.7,[16] and the interaction network was visualized using Cytoscape (Institute for Systems Biology, Seattle, Washington, USA, version 3.10.2, https://cytoscape.org/).[17,18] Key nodes were identified based on network topology parameters exceeding the median, including maximal clique centrality, degree, closeness, and betweenness.[19,20] Kyoto Encyclopedia of Genes and Genomes (updated 2024-09-01, https://www.kegg.jp/) functional enrichment analysis was performed using the Database for Annotation, Visualization, and Integrated Discovery (DAVID, updated 2024-07-05, https://david.ncifcrf.gov/) with a significance threshold of $P < 0.05$. For gene expression analysis, GSEA was conducted and visualized using R (R Foundation for Statistical Computing, Vienna, Austria) packages including "org.Hs.eg.db," "clusterProfiler," and "pathview." Subsequently, co-expression network analysis was performed using weighted gene co-expression network analysis with the R package "corrplot" applying thresholds of $P < 0.05$ and Pearson correlation coefficient >0.8.

2.3. Virus preparation

IAV (H1N1) strain A/PR/8/34 was obtained from the American Type Culture Collection (ATCC, VR-95 Manassas, Virginia, USA), propagated in chicken embryos, and stored at −80 °C. Viral titers were determined using the chicken hemagglutination assay, and the median lethal dose (LD_{50}) was calculated.[21]

2.4. Establishment of acute lung injury model

For all infections, mice were lightly anesthetized with isoflurane and administered PR8 virus intranasally in 35 μL of normal saline. Mice received 5 LD_{50} of the virus via intranasal drops. Body weights were measured on days 0, 3, and 5 postinfection (dpi). On day 5, mice were euthanized in accordance with institutional guidelines, and samples were collected for subsequent analyses.

2.5. Animal experiments

A total of 38 C57BL/6JNifdc male and female mice (5-week-old, [14.00 ± 1.00] g) were obtained from the National Institutes for Food and Drug Control. The study was approved by the Institutional Animal Care and Use Committee of the National Institutes for Food and Drug Control, Beijing, China [Approval No. 2023(B) 063]. All mice were randomly assigned to experimental groups based on body weight to ensure uniform infection efficiency. Data from 2 batches of animals were pooled for the final analysis of each experiment. Batch 1 included 2 groups to evaluate findings from the multinetwork analysis: Mock (n = 10; 5 males and 5 females) and IAV (n = 10; 5 males and 5 females). Batch 2 included 3 groups to assess the role of toll-like receptor 3 (TLR3) in IAV infection: Mock (n = 6; 3 males and 3 females), IAV (n = 6; 3 males and 3 females), and TLR3 inhibitor (n = 6; 3 males and 3 females). Baseline health status and body weight were assessed, and characteristics were generally consistent across groups. All animals were housed in an animal biosafety level 2 (ABSL-2) containment facility at (24 ± 1) °C with a 12-hour light/dark cycle and had *ad libitum* access to standard rodent chow and water.

The TLR3 inhibitor ODN 24991 sodium (MedChemExpress, Monmouth Junction, New Jersey, USA, HY-150746A) was dissolved in saline and administered at a dose of 1 mg/kg via intraperitoneal injection 1 hour before IAV infection. All animals in

each group were used for serum factor analysis. Whole lung tissue samples were equally divided for histopathological evaluation and protein- or RNA-based molecular analyses.

2.6. Lung index and histology

The lung index was calculated as the ratio of lung weight to body weight. Hematoxylin–eosin (H&E) staining (Pinuofei Biotechnology, Wuhan, China, S191003) was performed to assess lung injury. Briefly, lung tissues were fixed in 4% paraformaldehyde for 24 hours, dehydrated through a graded alcohol series, cleared with xylene, and embedded in paraffin. The paraffin blocks were mounted on a microtome and sectioned at 4 to 6 μm. Sections were stained with H&E, and pathological changes in lung tissue across different groups were evaluated by 2 trained observers blinded to the experimental groups. Each slide was scored based on the severity of histologic changes, including inflammation, interstitial pneumonia, edema, alveolitis, bronchiolitis, alveolar destruction, mononuclear cell infiltration, pulmonary hemorrhage, and peribronchiolar inflammation.[22] The scoring system was as follows: no pathological changes = 0; mild = 1; moderate = 2; severe = 3; extremely severe = 4. The acute lung injury model was confirmed by H&E staining and lung injury scoring.

2.7. RNA isolation and real-time quantitative polymerase chain reaction (PCR)

Total RNA was extracted from lung tissue using TRIzol (Tiangen Biochemical Technology Co., Ltd., Beijing, China, A1212A01). RNA samples were reverse-transcribed into cDNA using FastKing gDNA Dispelling RT SuperMix (Tiangen Biochemical Technology Co., Ltd., Beijing, China, B0516A). Real-time quantitative PCR was performed using Taq Pro Universal SYBR qPCR Master Mix (Vazyme Biotech Co., Ltd., Nanjing, China, 7E1081B5). The reaction conditions were as follows: 95 °C for 30 seconds, followed by 40 cycles of 95 °C for 10 seconds and 60 °C for 30 seconds, in a total volume of 20 μL. Primer sequences are listed in Supplemental Table S1, https://links.lww.com/STCM/A69. Relative mRNA expression was normalized to β-actin and calculated using the $2^{-\Delta\Delta Ct}$ method.

2.8. Enzyme-linked immunosorbent assay (ELISA)

At 5 dpi, blood was collected and allowed to clot at room temperature for 2 hours, followed by centrifugation at 12,000 r/min at 4 °C for 15 minutes to collect the supernatant. Serum concentrations of cytokines, chemokines, and interferons (IFNs) were measured using ELISA kits according to the manufacturers' instructions. All ELISA kits were purchased from Shanghai Enzyme-linked Biotechnology Co. (Shanghai, China) and included mouse C-C motif chemokine ligand (CCL)-2, CCL-5, CCL-10, interleukin (IL)-18, IL-6, tumor necrosis factor-alpha (TNF-α), IFN-α, IFN-β, and IFN-γ (Supplemental Table S2, https://links.lww.com/STCM/A69). Additionally, serum levels of IFN-γ, CCL-5, IL-6, and TNF-α were measured using the ABplex Mouse 4-Plex Custom Panel (ABclonal, Wuhan, China, RK04381).

2.9. Western blotting analysis

Following radioimmunoprecipitation assay (RIPA) lysis, total protein was extracted and quantified using the bicinchoninic acid (BCA) method (Beyotime Biotechnology Co., Ltd., Shanghai, China, P0012). Western blotting analysis was performed according to protocols described in our previous studies.[23–26] Antibodies against TLR3 (Affinity Biosciences, Changzhou, China, DF6415, 1:1000 dilution), p-MLKL (ABclonal Technology, Wuhan, China, AP0949, 1:1000 dilution), MLKL (Proteintech, Wuhan, China, 66675-1-Ig, 1:1000 dilution), p-RIPK3 (ABclonal Technology, Wuhan, China, AP1260, 1:1000 dilution), and RIPK3 (ABclonal Technology, Wuhan, China, A5431, 1:1000 dilution) were used as listed in Supplemental Table S3, https://links.lww.com/STCM/A69. Beta-actin (rabbit Anti-β-actin, Bioss Biotechnology, Beijing, China, bs-0061R, 1:5000 dilution) served as a loading control for lung tissue samples.

2.10. Immunofluorescence staining

Double and triple immunofluorescence staining was performed as previously described.[27] Primary antibodies to rabbit Emerin and mouse Lamin B1 were used for Emerin/Lamin B1 double staining (Proteintech, Wuhan, China; 66095-1-1g and 10351-1-AP; 1:200 dilution). Primary antibodies to rabbit citrullinated histone H3 (Cit-H3), mouse myeloperoxidase (MPO), and rabbit eukaryotic nucleoprotein (NP) were used for Cit-H3/MPO/NP triple staining (Proteintech, Wuhan, China; 66177-1-1g, 13754-1-AP, and 18009-1-AP; 1:200, 1:400, and 1:200 dilution). Sections were incubated with FITC- (488 nm), CY3- (555 nm), and CY5- (647 nm) conjugated secondary antibodies (SeraCare, Beijing, China; 5220-0336 and 5220-0341; 1:400 dilution) for 2 hours at room temperature, protected from light. Nuclei were counterstained with 4',6-diamidino-2-phenylindole (Beyotime Biotechnology, Shanghai, China, C1006) for 4 minutes at room temperature. Stained sections were visualized and imaged using a confocal microscope (Abberior, Göttingen, Germany) and Pannoramic Scan II (3DHISTECH, Budapest, Hungary). All antibodies used are listed in Supplemental Table S3, https://links.lww.com/STCM/A69. Reagents and instruments involved in the experiment are listed in Supplemental Tables S4 and S5, https://links.lww.com/STCM/A69.

2.11. Statistical analyses

Statistical analyses were performed using GraphPad Prism 8.0 software (San Diego, California, USA). Data are expressed as the mean ± standard deviation and were analyzed using analysis of variance with Sidak multiple comparisons test for comparisons across multiple groups, and an unpaired *t* test for comparisons between 2 groups. Differences were considered statistically significant when the *P* value was less than 0.05.

3. Results

3.1. The imbalance of the "immune-inflammation" system is closely related to the pathogenesis of IAV infection

To identify candidate targets underlying the pathogenesis of IAV infection, data mining was performed on transcriptome data from the GEO database (GEO No. GSE163959). A total of 1113 IAV-related genes were identified in lung tissues, including 707 upregulated genes and 406 downregulated genes, based on the criteria of a *t* test $P < 0.05$ and $|\text{fold change}| > 1$.

The heatmap of DEGs is shown in Figure 1A, suggesting a clear separation between the IAV-infected and mock-infected groups. A PPI network of IAV-related genes was then constructed based on gene interactions (combined score > 0.7) as described in our previous studies.[19,20] The network consisted of 283 nodes and 1691 interactions. Based on network topology parameters, including "degree," "closeness," and "betweenness," 93 hub genes were identified (median values: degree = 4.0000, closeness = 85.2524, betweenness = 35.4127). These hub genes were involved in multiple biological pathways, including immune-inflammation regulation, signal transduction, and cellular processes (Fig. 1B). Notably, IAV infection upregulated multiple biological pathways, particularly canonical immune and inflammatory pathways, which are closely associated with the progression of IAV infection.[28]

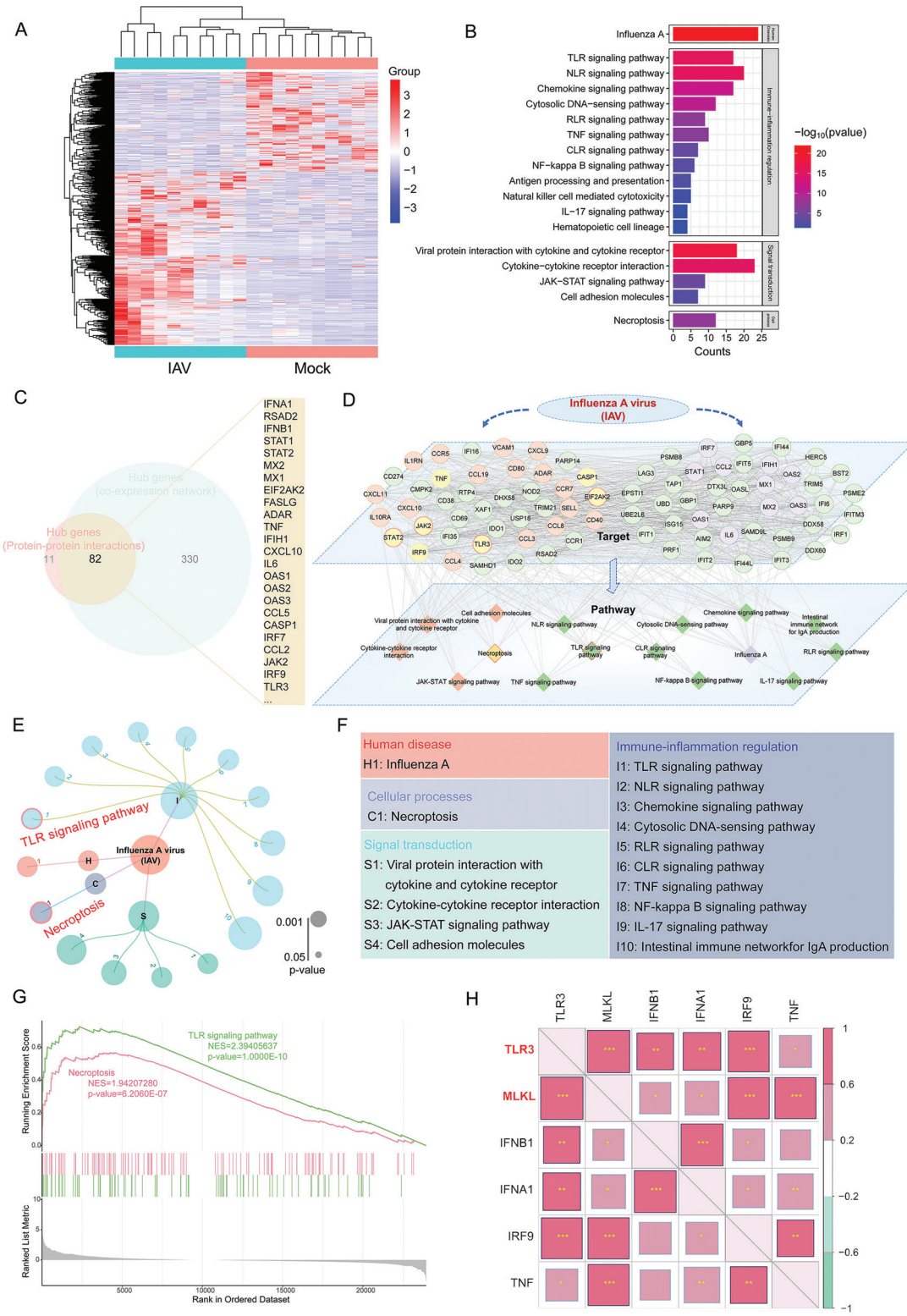

Figure 1. Molecular mechanisms of influenza A virus (IAV) infection based on a series of bioinformatics analyses. (A) Heatmap of transcriptome microarray data from lung tissue in database GSE163959. (B) KEGG enrichment analysis of all differentially expressed genes (DEGs). (C) Candidate gene sets identified from the intersection between protein–protein interaction (PPI) and co-expression networks. (D) Subnetwork of the "IAV infection-related gene-pathway" network constructed based on the links among DEGs. Circles represent IAV infection-related genes, and diamonds represent enriched pathways. Green nodes are closely associated with "immune-inflammation" system imbalance regulation; orange nodes with signal transduction; yellow nodes with cellular processes; and purple nodes with human diseases. Circles or diamonds outlined in red indicate potential targets and candidate pathways. (E) Three-layer circular network of intersecting genes from the PPI and co-expression networks. (F) Functional module enrichment analysis of the intersecting genes. (G) Gene set enrichment analysis (GSEA) showing enrichment of the necroptosis and toll-like receptor (TLR) signaling pathways in IAV-infected versus mock-infected groups. (H) Heatmap of correlations between the IAV-infected and mock groups. *$P < 0.05$, **$P < 0.01$, ***$P < 0.001$ versus the IAV-infected group. In the correlation heatmap, pink indicates positive correlations, while green represents negative correlations, and color intensity corresponds to gene expression levels. KEGG, Encyclopedia of Genes and Genomes.

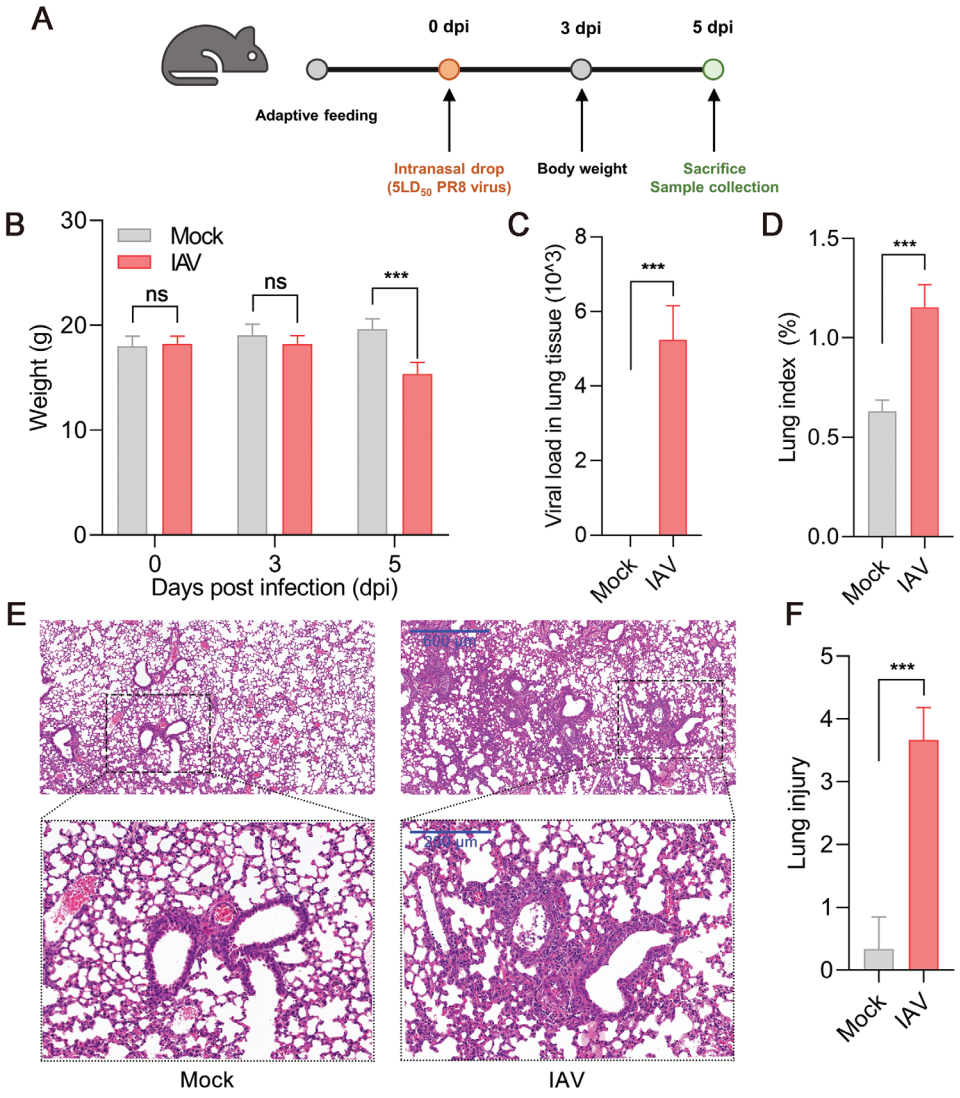

Figure 2. Assessment of disease severity in the IAV-PR8 virus-induced acute lung injury mouse model. (A) Experimental schedule. (B) Changes in body weight over 5 days following IAV-PR8 infection (n = 10 per group; ANOVA with Sidak multiple comparisons test). (C) Viral RNA load analyzed from total RNA extracted from lung tissues (n = 6 per group; unpaired t test). (D) Lung index (n = 10 per group; unpaired t test). (E) Histopathological changes in lung tissues collected on day 5 postinfection detected by H&E staining. (F) Quantification of lung injury based on histopathological analysis of H&E-stained sections (n = 6 per group; unpaired t test). Data are presented as mean ± SD. All experiments were performed in triplicate. $^{***}P < 0.001$; ns ≥ 0.05. Scale bar represents 600 and 200 μm, respectively. ANOVA, analysis of variance; H&E, hematoxylin–eosin; IAV, influenza A virus; ns, not significant; SD, standard deviation.

Subsequently, a co-expression network was constructed using the links of the gene expression across tissues, comprising 826 nodes and 32,907 significant co-expression correlations (P < 0.05, Pearson correlation coefficient >0.8). Using the degree parameter, 412 hub genes were screened (median degree = 22). Overall, 82 overlapping genes between the PPI and co-expression networks were selected as candidate genes for further bioinformatics analysis (Fig. 1C).

Next, a subnetwork of "IAV-infection-related genes-pathway" among DEGs was constructed, suggesting that the molecular mechanisms of IAV infection may involve the imbalance of the "immune-inflammation" system via TLR and necroptosis signaling pathways. Candidate genes were selected based on their topological importance, such as TNF-α, IL-6, CCL-5, and TLR3 (Fig. 1D). A 3-layer circular network of the intersection genes showed that IAV infection was strongly associated with dysregulation of the "immune-inflammation" system, such as TLR, NOD-like receptor, retinoic acid-inducible gene I-like receptor (RLR), and C-type lectin receptor signaling pathways, cellular processes (necroptosis), and signal transduction pathways, including Janus kinase-signal transducer and activator of transcription (JAK-STAT) (Fig. 1E, 1F). Among these, the TLR signaling pathway and necroptosis occupied central positions within the network cluster. GSEA was performed using P values and normalized enrichment scores (NES) to assess statistical significance (Fig. 1G), corroborating the functional enrichment results (TLR signaling pathway: NES = 2.3941, $P = 1.00 \times 10^{-10}$; necroptosis: NES = 1.9421, $P = 6.21 \times 10^{-7}$), demonstrating activation of TLR and necroptosis pathways following IAV challenge. Figure 1H showed that TLR3 and MLKL may regulate the expression of other genes at the transcriptional level (all P < 0.05, Pearson correlation coefficient >0.8). Innate immune responses to IAV infection are partially initiated by TLR3, [29] suggesting that TLR3 activation could act upstream of necroptosis in IAV pathogenesis. Moreover, excessive TLR expression is known to trigger an active inflammatory response and activate the downstream nuclear factor kappa-B signaling pathway. Based on these findings, we hypothesize that TLR3-mediated necroptosis signaling represents a key molecular mechanism in the pathogenesis of influenza.

3.2. IAV triggers TLR3-mediated necroptosis via regulating RIPK3/MLKL signaling

To validate the findings from the bioinformatics analyses, *in vivo* experiments were performed using a mouse model of acute lung injury induced by IAV (H1N1) strain A/PR/8/34 (PR8) (Fig. 2A). The average body weight of mice reached its lowest point on day 5 after infection ($P < 0.001$, Fig. 2B), after which the mice were euthanized, and viral load in lung tissues was assessed by viral RNA real-time quantitative PCR. As shown in Fig. 2C and 2D, both viral load and lung indexes were significantly increased in IAV-infected mice compared with the mock-infected group (all $P < 0.001$). Lung histopathology was evaluated using H&E staining, and semiquantitative analysis was performed to determine the degree of histologic changes.[22] In the mock-infected group, lung tissue exhibited normal alveolar cavities, thin alveolar walls, and no edema or hemorrhage. In contrast, IAV infection induced alveolar structural damage, thickened alveolar walls, pulmonary congestion, and inflammatory cell infiltration (Fig. 2E). Semiquantitative scoring confirmed the occurrence of acute lung injury, consistent with the histopathological observation ($P < 0.001$, Fig. 2F).

Our network-based analyses suggested that TLR3-mediated necroptosis signaling may underlie the pathogenesis of influenza. Lamins are important caspase substrates and key components of the nuclear lamina,[30,31] and loss of nuclear Lamin B1 disrupts the integrity of the nuclear envelope.[32] To examine nuclear membrane morphology, lamin cleavage, and structural integrity in lung tissues of IAV-PR8-infected mice, immunofluorescence microscopy was performed.[33] Imaging of the nuclear lamina protein Lamin B1 and the inner nuclear membrane protein Emerin revealed ovoid nuclei with well-defined boundaries in mock-infected mice. In contrast, IAV-PR8 infection induced large gaps in Lamin B1 staining and breaches in the Emerin signal (Fig. 3A). Consistently, the fluorescence intensity detected from each emission channel was significantly decreased (all $P < 0.01$, Fig. 3B), indicating reduced Lamin B1 and Emerin protein levels.

To our knowledge, MLKL is a critical substrate of RIPK3, and phosphorylation of MLKL (p-MLKL) represents a key event in necroptosis.[34–36] We examined key necroptosis mediators and downstream effector molecules in lung tissues following viral infection (Fig. 3C). Consistent with previous observation, TLR3 protein expression in lung tissues was significantly increased after IAV-PR8 infection ($P < 0.01$, Fig. 3D). Additionally, the protein levels of key necroptosis components, including p-MLKL/MLKL and p-RIPK3/RIPK3, were markedly elevated in IAV-PR8-infected mice ($P < 0.05$ and $P < 0.01$, respectively; Fig. 3E, 3F). These findings indicated that TLR3 may mediate activation of RIPK3/MLKL, subsequently contributing to nuclear envelope damage during IAV infection.

3.3. IAV infection drives neutrophil recruitment and induces inflammatory response

To investigate the role of TLR3-mediated necroptosis in IAV-induced inflammatory responses *in vivo*, proinflammatory factors and mediators were measured using ELISA. Notably, IFN-α, IFN-β, and IFN-γ protein levels were significantly elevated ($P < 0.001$, $P < 0.01$, and $P < 0.001$, respectively; Fig. 4A). Type I interferons, including IFN-α and IFN-β, induce the expression of interferon-stimulated genes that confer antiviral activity to host cells. However, aberrant activation can exacerbate inflammation and autoimmunity.[37] Cytokines and chemokines play critical roles in shaping adaptive immunity during viral infection.[38,39] Consistently, the serum levels of chemokines were markedly upregulated in IAV-PR8-infected mice, including CCL-2, CCL-5, and CCL-10 ($P <$

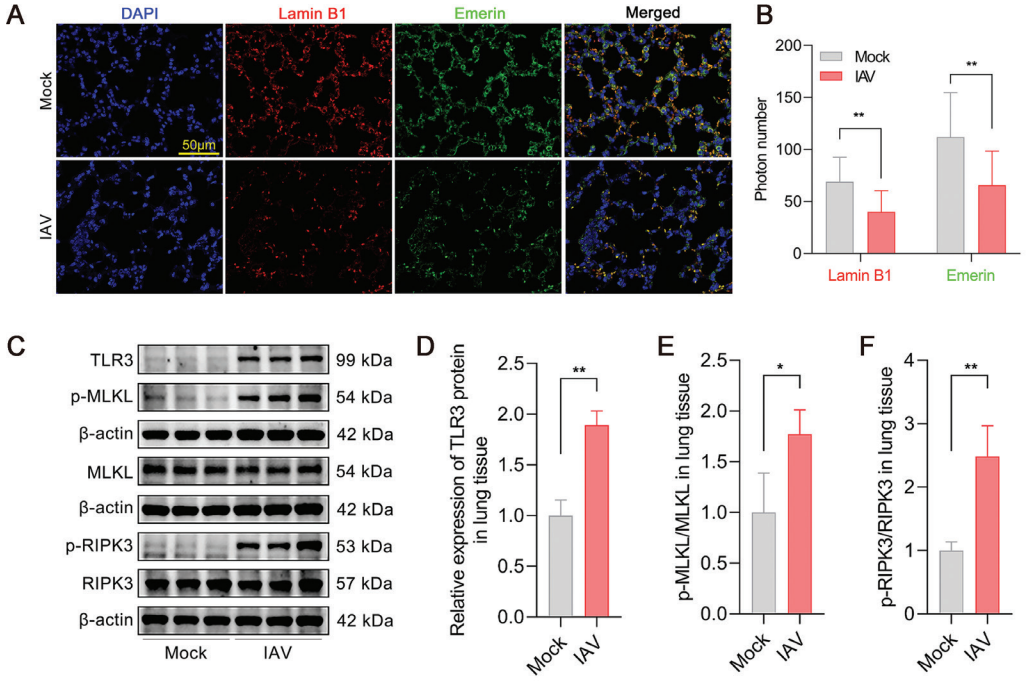

Figure 3. IAV-PR8 infection induces necroptosis via the TLR3/RIPK3/MLKL signaling pathway regulation. (A) Examination of nuclear envelope integrity using antibodies against Lamin B (red) and Emerin (green). Nuclei were stained with DAPI (blue). (B) Quantification of Lamin B1 and Emerin fluorescence intensity using confocal microscopy (n = 6 per group; ANOVA with Sidak multiple comparisons test). (C) Protein expression levels of TLR3, p-MLKL, MLKL, p-RIPK3, and RIPK3 in lung tissues of IAV-PR8 virus-infected mice analyzed by Western blotting. (D) Semiquantitative analysis of TLR3 protein expression in lung tissues (n = 3 per group; unpaired *t* test). (E) Semiquantitative analysis of p-MLKL/MLKL in lung tissues (n = 3 per group; unpaired *t* test). (F) Semiquantitative analysis of p-RIPK3/RIPK3 in lung tissues (*n* = 3 per group; unpaired *t* test). Data are presented as mean ± SD. All experiments were performed in triplicate. **P* < 0.05, ***P* < 0.01. ANOVA, analysis of variance; DAPI, 4',6-diamidino-2-phenylindole; IAV, influenza A virus; MLKL, mixed lineage kinase domain-like protein; SD, standard deviation; TLR3, toll-like receptor 3.

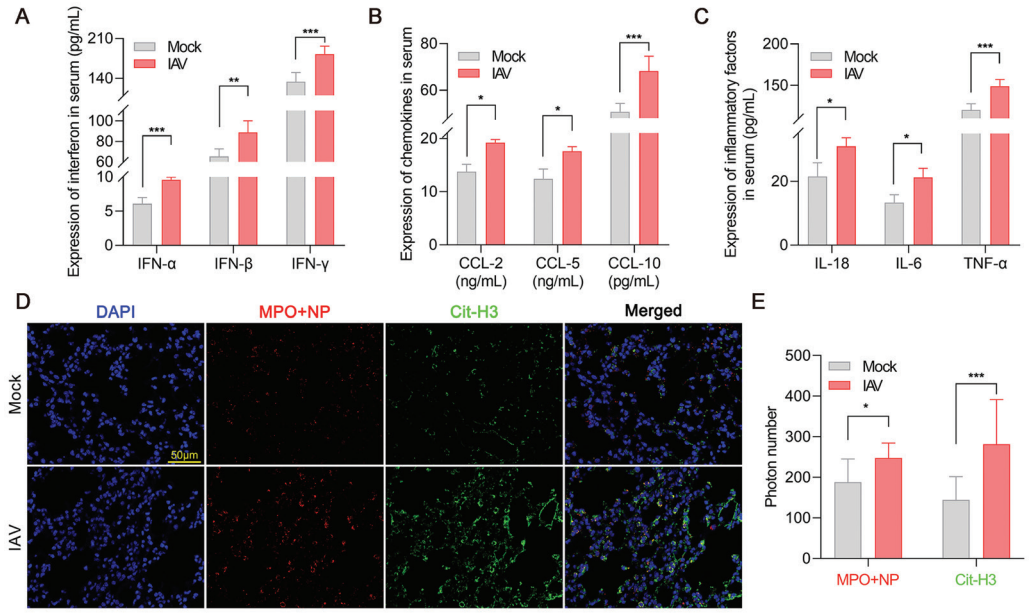

Figure 4. IAV-PR8 infection activates the inflammatory response through TLR3-mediated necroptosis. (A) Expression levels of IFN-α, IFN-β, and IFN-γ proteins in the sera of IAV-PR8 virus-infected mice determined by ELISA (n = 6 per group; ANOVA with Sidak multiple comparisons test). (B) Expression levels of CCL-2, CCL-5, and CCL-10 proteins in the sera of IAV-PR8 virus-infected mice determined by ELISA (n = 6 per group; ANOVA with Sidak multiple comparisons test). (C) Expression levels of IL-18, IL-6, and TNF-α proteins in the sera of IAV-PR8 virus-infected mice determined by ELISA (n = 6 per group; ANOVA with Sidak multiple comparisons test). (D) Immunofluorescence staining of lung tissues from IAV-PR8-infected and mock-infected mice showing neutrophils (MPO) and NP (MPO-NP, red) as well as NETs (Cit-H3, green). Nuclei were stained with DAPI (blue). (E) Quantification of MPO+NP/Cit-H3 fluorescence intensity using confocal microscopy (n = 3 per group; ANOVA with Sidak multiple comparisons test). Data are presented as mean ±SD. All experiments were performed in triplicate. $^{*}P < 0.05$, $^{**}P < 0.01$, $^{***}P < 0.001$. ANOVA, analysis of variance; CCl, chemokine ligand; DAPI, 4',6-diamidino-2-phenylindole; ELISA, enzyme-linked immunosorbent assay; IAV, influenza A virus; IFN, interferon; IL, interleukin; MPO, myeloperoxidase; NET, neutrophil extracellular trap; NP, eukaryotic nucleoprotein; SD, standard deviation; TLR3, toll-like receptor 3; TNF-α, tumor necrosis factor-alpha.

0.05, $P < 0.05$, and $P < 0.001$, respectively; Fig. 4B). Furthermore, key inflammatory cytokines associated with necroptosis (IL-18, IL-6, and TNF-α) were also elevated in the sera of IAV-infected mice ($P < 0.01$, $P < 0.05$, and $P < 0.001$, respectively; Fig. 4C).

Notably, IAV infection induces neutrophil infiltration, a hallmark of IAV-induced pathology,[40,41] and stimulates neutrophil extracellular trap (NET) formation by human neutrophils *in vitro* via a distinctive pathway.[42] To determine whether these pathological changes were associated with neutrophil infiltration and NET formation, immunofluorescence staining was performed to assess neutrophil infiltration (MPO, a known NET marker) and the expression of Cit-H3 (a NET-specific marker).[43,44] Consistent with these findings, IAV-PR8 infection significantly increased neutrophil infiltration (MPO, $P < 0.05$) and NET formation (Cit-H3, $P < 0.001$) in lung tissues (Fig. 4D, 4E). These results indicate that IAV infection promotes neutrophil infiltration and NET formation, contributing to subsequent inflammatory responses in both innate and adaptive immunity.

3.4. TLR3 plays a key role in activating necroptosis signaling during IAV infection

To determine whether TLR3 directly mediates necroptosis, the TLR3 inhibitor ODN 24991 sodium was administered during IAV infection. Treatment with the TLR3 inhibitor significantly attenuated body weight loss ($P < 0.01$, Fig. 5A). In IAV-infected mice, severe alveolar septal thickening, consolidation, pulmonary edema, and infiltration of inflammatory immune cells were observed. These pathological changes were significantly alleviated by the TLR3 inhibitor ($P < 0.001$, Fig. 5B, 5C). In terms of inflammation, TLR3 inhibition markedly reduced serum levels of IFN-γ, CCL-5, IL-6, and TNF-α ($P < 0.001$, $P < 0.05$, $P < 0.001$, and $P < 0.05$, respectively; Fig. 5D–5G). Moreover, the large gaps in Lamin B1 staining and breaches in the Emerin signal induced by IAV were ameliorated following TLR3 inhibition ($P < 0.05$ and $P < 0.001$, respectively; Fig. 5H, 5I). IAV infection increased NP levels and promoted NET formation, as evidenced by elevated MPO and Cit-H3 in lung tissues, which were reversed by TLR3 inhibitor treatment (all $P < 0.001$; Fig. 5J, 5K). Western blotting analysis revealed that the elevated protein levels of TLR3, p-MLKL/MLKL, and p-RIPK3/RIPK3 were significantly downregulated in the TLR3 inhibitor group ($P < 0.01$, $P < 0.05$, and $P < 0.05$, respectively; Fig. 5L, 5M).

4. Discussion

Accumulating evidence shows that IAV infection causes necroptosis in both infiltrating immune cells and lung structural alveolar epithelial cells.[2,45] The current study, an integrative approach combining gene expression profiling, multinetwork analysis, GSEA, and experimental validations, identified TLR3-mediated RIPK3-MLKL signaling-induced necroptosis as a key underlying molecular mechanism for regulating the imbalance network of the "immune-inflammation" network during IAV infection. Clinical studies and mouse models have demonstrated that severe H1N1 infection is associated with rapidly progressive pneumonia, extensive and diffuse alveolar damage, acute respiratory distress syndrome, and, in some cases, multiorgan failure, contributing to high mortality.[46,47] IAV can directly infect and damage lung epithelial cells and alveolar macrophages, triggering immune responses and acute lung injury, which result in pulmonary edema and impaired alveolar fluid clearance. Our data indicate that excessive immune response-induced immunopathological damage plays a critical role in the pathogenesis of acute lung injury.

Double-stranded RNAs are produced in virus-infected cells during replication and play a crucial role in eliciting antiviral responses by binding to TLR3, a member of the pattern recognition receptor family, and RLRs.[48,49] Combined treatment

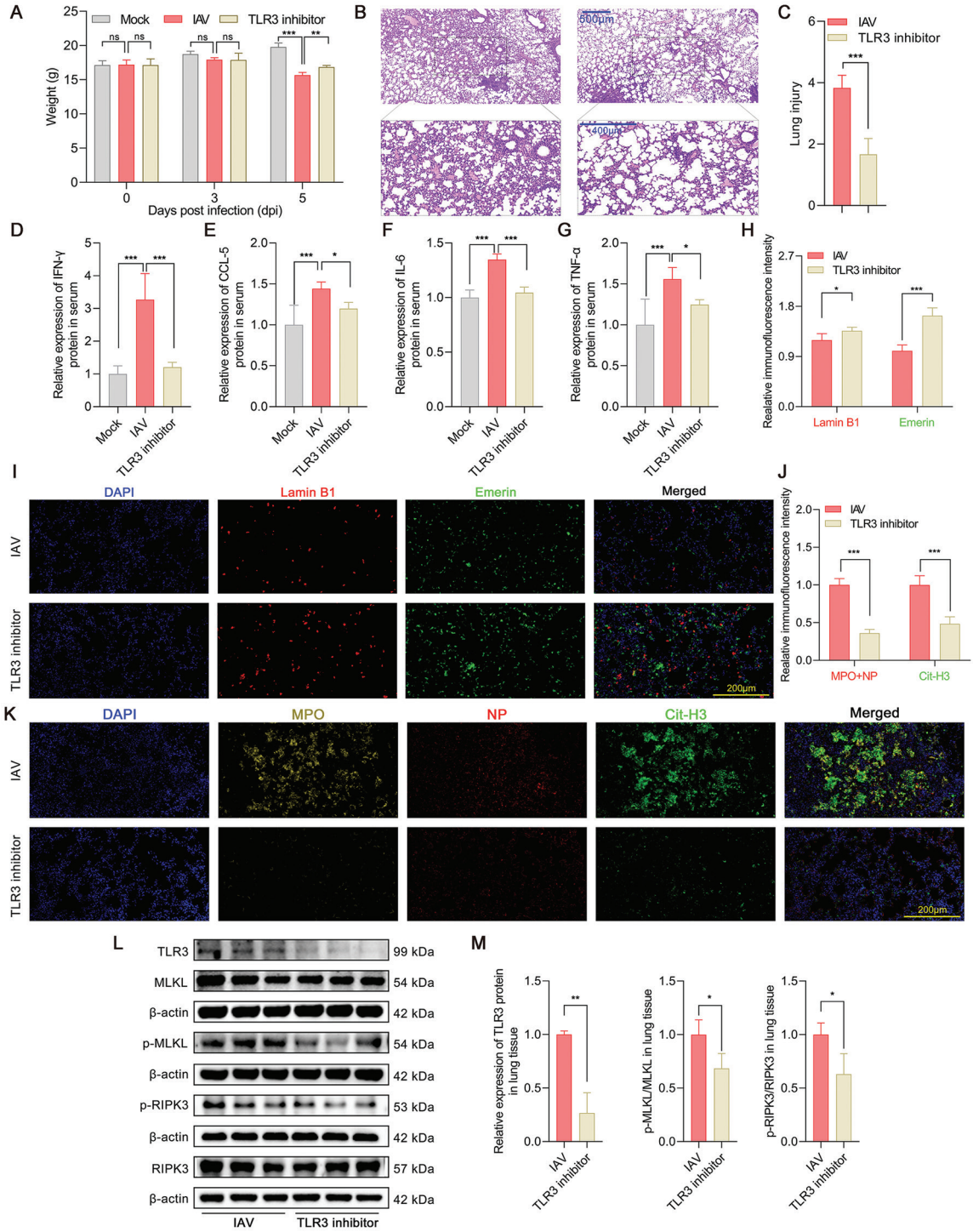

Figure 5. Effects of TLR3 on RIPK3-MLKL-mediated necroptosis during IAV infection. (A) Changes in body weight over 5 days following IAV-PR8 infection (n = 6 per group; ANOVA with Sidak multiple comparisons test). (B) Histopathological changes in lung tissues collected on day 5 postinfection detected by H&E staining. (C) Quantification of lung injury based on histopathological analysis of H&E-stained sections (n = 6 per group; unpaired t test). (D–G) Expression levels of IFN-γ, CCL-5, IL-6, and TNF-α proteins in serum determined using the ABplex Mouse 4-Plex Custom Panel (n = 6 per group; ANOVA with Sidak multiple comparisons test). (H) Relative immunofluorescence intensities of Lamin B1 and Emerin analyzed using the Pannoramic Scan II system (n = 6 per group; ANOVA with Sidak multiple comparisons test). (I) Examination of nuclear envelope integrity using antibodies against Lamin B (red) and Emerin (green); nuclei were counterstained with DAPI (blue). (J) Relative immunofluorescence intensities of MPO+NP and Cit-H3 measured using the Pannoramic Scan II system (n = 3 per group; ANOVA with Sidak multiple comparisons test). (K) Immunofluorescence staining of lung tissues showing neutrophils (MPO, yellow), NP (red), and NETs (Cit-H3, green); nuclei were stained with DAPI (blue). (L) Protein expression levels of TLR3, p-MLKL, MLKL, p-RIPK3, and RIPK3 in lung tissues analyzed by Western blotting. (M) Semiquantitative analysis of TLR3, p-MLKL/MLKL, and p-RIPK3/RIPK3 in lung tissues (n = 3 per group; unpaired t test). Data are presented as mean ± SD. All experiments were performed in triplicate. $^{*}P < 0.05$, $^{**}P < 0.01$, $^{***}P < 0.001$, ns ≥ 0.05. ANOVA, analysis of variance; CCL, chemokine ligand; Cit-H3, citrullinated histone H3; H&E, hematoxylin–eosin; IAV, influenza A virus; ; IFN, interferon; IL, interleukin; MLKL, mixed lineage kinase domain-like protein; MPO, myeloperoxidase; NET, neutrophil extracellular trap; NP, eukaryotic nucleoprotein; ns, not significant; TLR3, toll-like receptor 3; TNF-α, tumor necrosis factor-alpha.

with sirolimus and oseltamivir attenuates H1N1-induced severe lung injury, which correlates with suppression of the mTOR-NLRP3-IL-1β axis and a reduced viral titer.[47] TLR3 and RLRs activate multiple signaling pathways, including nuclear factor kappa-B and mitogen-activated protein kinase signaling, leading to the production of proinflammatory cytokines and induction of interferon-stimulated genes through transcriptional regulation. IAV induces cytokine storm via IFN regulation, resulting in tissue damage and ultimately lung injury.[50] Concurrently, double-stranded RNA is also produced in stressed, apoptotic, or necrotic cells.[51,52] Our research showed increased expression of TLR3 protein in IAV-infected lung tissues, which subsequently induces proinflammatory cytokines, such as IFNs and ILs, contributing to the hyperinflammatory response. Programmed cell death, particularly necroptosis, participates in the pathogenesis of several diseases, including influenza.[53,54] Necroptosis is characterized by RIPK3 phosphorylation and the RIPK3-mediated phosphorylation of MLKL.[55–57] While programmed cell death is an effective mechanism for IAV clearance, eliminating infected cells, limiting viral spread, and activating adaptive immunity, necroptotic cell debris is highly immunogenic and promotes neutrophil recruitment and activation. Neutrophils, in turn, can trigger a pathogenic feed-forward inflammatory response during IAV infection, as the nucleus contains numerous damage-associated molecular patterns, including DNA.[2] Our data implicate MLKL-mediated necroptosis as a driver of IAV virulence. Importantly, the TLR3 inhibitor ameliorated IAV-induced acute lung injury by suppressing MLKL-mediated necroptosis. These findings identify TLR3-RIPK3-MLKL-mediated necroptosis as a potential therapeutic target in severe influenza.

While the use of specific pharmacological inhibitors provides strong functional evidence supporting the proposed pathway, future studies employing cell-specific conditional knockout models will be valuable to validate these findings and rule out potential off-target effects of the compounds used. This study has several limitations: (1) the transcriptome data were obtained from the GEO database, and we did not perform a comprehensive transcriptome analysis of mouse lungs infected with the IAV-PR8; (2) the therapeutic potential of targeting TLR3-RIPK3-MLKL-mediated necroptosis, including candidate drugs or signal interventions, requires further investigation.

5. Conclusions

In this study, we provide both network-based and *in vivo* evidence that TLR3-RIPK3-MLKL-mediated necroptosis may be an underlying molecular mechanism of IAV infection-induced acute lung injury. These findings offer new insights into the pathogenesis of IAV infection and may promote the research on the mechanism of TCM against influenza virus and provide actionable drug targets for natural product screening.

Acknowledgments

All authors of this manuscript sincerely thank their respective universities and institutes for their technical assistance and invaluable support throughout the completion of this research project. We also extend our gratitude to Prof. Amos Panet and Dana G Wolf, Department of Clinical Microbiology and Infectious Diseases, Hadassah University Hospital, for submitting the RNA-seq data to the National Center for Biotechnology Information (NCBI) Gene Expression Omnibus (GEO) database.

Statement of ethics

The study was approved by the Institutional Animal Care and Use Committee of the National Institutes for Food and Drug Control, Beijing, China (Approval No. 2023(B) 063). All procedures were strictly conducted in accordance with the guidelines and regulations for the use and care of the animal biosafety level 2 laboratory. Animals were handled following the ethical requirements of the People's Republic of China, with every effort made to minimize animal suffering. All experiments, including treatment, anesthesia, and euthanasia, were performed in compliance with the ARRIVE guidelines (https://www.nc3rs.org.uk/arrive-guidelines).

Conflict of interest statement

The authors declare that they have no conflicts of interest with regard to the content of this report.

Funding source

This study was funded by the National Key R&D Program of China (2023YFC3502900 and 2023YFC2308200), the National Natural Science Foundation of China (82304830), the Fundamental Research Funds for Central Public Welfare Research Institutes (ZZ16-YQ-026, ZXKT24003, ZXKT23008, and ZXKT22054), and the Scientific and Technological Innovation Project of the China Academy of Chinese Medical Sciences (CI2023E002 and CI2023C013YL).

Data availability statement

The datasets analyzed in this study were obtained from the National Center for Biotechnology Information Gene Expression Omnibus (GEO) under accession number GSE163959.

Author contributions

Haiyu Xu and Lijuan Song coordinated the study. Weijie Li designed and performed the experimental validation and wrote and revised the manuscript. Congying Huang, Ziling Zeng, Xiang Li, Jia Xu, Tian Gong, Hao Zhang, Xinyan Zhang, Ping Wang, and Yuanjia Hu performed experiments and/or contributed to discussions. All authors participated in manuscript revision and approved the final version.

References

[1] D'Angiolella LS, Lafranconi A, Cortesi PA, Rota S, Cesana G, Mantovani LG. Costs and effectiveness of influenza vaccination: a systematic review. *Ann Ist Super Sanita* 2018;54:49–57.
[2] Zhang T, Yin C, Boyd DF, et al. Influenza virus Z-RNAs induce ZBP1-mediated necroptosis. *Cell* 2020;180:1115–1129.e13.
[3] Kalil AC, Thomas PG. Influenza virus-related critical illness: pathophysiology and epidemiology. *Crit Care* 2019;23:258.
[4] Sah P, Medlock J, Fitzpatrick MC, Singer BH, Galvani AP. Optimizing the impact of low-efficacy influenza vaccines. *Proc Natl Acad Sci USA* 2018;115:5151–5156.
[5] Groenewold MR, Burrer SL, Ahmed F, Uzicanin A, Luckhaupt SE. Health-related workplace absenteeism among full-time workers — United States, 2017–2018 influenza season. *MMWR Morb Mortal Wkly Rep* 2019;68:577–582.
[6] Du Z, Nugent C, Galvani AP, Krug RM, Meyers LA. Modeling mitigation of influenza epidemics by baloxavir. *Nat Commun* 2020;11:2750.
[7] Oltean T, Ibanez LI, Divert T, et al. Reduced protection of RIPK3-deficient mice against influenza by matrix protein 2 ectodomain targeted active and passive vaccination strategies. *Cell Death Dis* 2022;13:280.
[8] Russell AB, Elshina E, Kowalsky JR, Te Velthuis AJW, Bloom JD. Single-cell virus sequencing of influenza infections that trigger innate immunity. *J Virol* 2019;93:e00500–e00519.
[9] Lee ACY, Zhang AJX, Chu H, et al. H7N9 influenza A virus activation of necroptosis in human monocytes links innate and adaptive immune responses. *Cell Death Dis* 2019;10:442.
[10] Jeon J, Noh HJ, Lee H, et al. TRIM24-RIP3 axis perturbation accelerates osteoarthritis pathogenesis. *Ann Rheum Dis* 2020;79:1635–1643.
[11] Grootjans S, Vanden Berghe T, Vandenabeele P. Initiation and execution mechanisms of necroptosis: an overview. *Cell Death Differ* 2017;24:1184–1195.

[12] Hanna-Addams S, Liu S, Liu H, Chen S, Wang Z. CK1α, CK1δ, and CK1ε are necrosome components which phosphorylate serine 227 of human RIPK3 to activate necroptosis. *Proc Natl Acad Sci USA* 2020;117:1962–1970.
[13] Sun L, Wang H, Wang Z, et al. Mixed lineage kinase domain-like protein mediates necrosis signaling downstream of RIP3 kinase. *Cell* 2012;148:213–227.
[14] Zhao J, Jitkaew S, Cai Z, et al. Mixed lineage kinase domain-like is a key receptor interacting protein 3 downstream component of TNF-induced necrosis. *Proc Natl Acad Sci USA* 2012;109:5322–5327.
[15] Alfi O, Yakirevitch A, Wald O, et al. Human nasal and lung tissues infected *ex vivo* with SARS-CoV-2 provide insights into differential tissue-specific and virus-specific innate immune responses in the upper and lower respiratory tract. *J Virol* 2021;95:e0013021.
[16] Szklarczyk D, Kirsch R, Koutrouli M, et al. The STRING database in 2023: protein-protein association networks and functional enrichment analyses for any sequenced genome of interest. *Nucleic Acids Res* 2023;51(D1):D638–D646.
[17] Shannon P, Markiel A, Ozier O, et al. Cytoscape: a software environment for integrated models of biomolecular interaction networks. *Genome Res* 2003;13:2498–2504.
[18] Otasek D, Morris JH, Bouças J, Pico AR, Demchak B. Cytoscape automation: empowering workflow-based network analysis. *Genome Biol* 2019;20:185.
[19] Li W, Wang K, Liu Y, et al. A novel drug combination of mangiferin and cinnamic acid alleviates rheumatoid arthritis by inhibiting TLR4/NFκB/NLRP3 activation-induced pyroptosis. *Front Immunol* 2022;13:912933.
[20] Li W, Mao X, Wu H, et al. Deciphering the chemical profile and pharmacological mechanisms of Baihu-Guizhi decoction using ultra-fast liquid chromatography-quadrupole-time-of-flight tandem mass spectrometry coupled with network pharmacology-based investigation. *Phytomedicine* 2020;67:153156.
[21] Wang X, Geng Z, Bao Y, et al. Shufeng Jiedu capsule alleviates influenza A (H1N1) virus induced acute lung injury by regulating the lung inflammatory microenvironment. *Heliyon* 2024;10:e33237.
[22] Lu M, Dravid P, Zhang Y, et al. A safe and highly efficacious measles virus-based vaccine expressing SARS-CoV-2 stabilized prefusion spike. *Proc Natl Acad Sci USA* 2021;118:e2026153118.
[23] Li W, Lu J, Mao X, et al. A comparative study on the mechanisms of two classical herbal formulae for rheumatoid arthritis applying cold and heat patterns based on target network. *Acta Pharm Sin* 2018;53(9):1387–1397.[in Chinese]
[24] Li W, Mao X, Wang X, et al. Disease-modifying anti-rheumatic drug prescription Baihu-Guizhi decoction attenuates rheumatoid arthritis via suppressing toll-like receptor 4-mediated NLRP3 inflammasome activation. *Front Pharmacol* 2021;12:743086.
[25] Li W, Zhang Y, Zhou S, et al. Clinical advantage staging and underlying mechanisms of Wangbi Tablets against knee osteoarthritis based on "disease-formula" interaction network. *China J Chin Mater Med* 2024;49(14):3924–3935.[in Chinese]
[26] Li W, Zhong Y, Gong T, et al. Underlying mechanisms of Huashi-Baidu formula against myocardial injury based on "transcriptome- putative target-phenotype gene" interactions. *Chin J Exp Tradit Med Form* 2024;30(22):69–78. [in Chinese]
[27] Guo Q, Li W, Wang C, et al. Biomolecular network-based synergistic drug combination discovery: a combination of paeoniflorin and liquiritin alleviates neuropathic pain by inhibiting neuroinflammation via suppressing the chemokine signaling pathway. *Signal Transduct Target Ther* 2020;5:73.
[28] Gunther RC, Bharathi V, Miles SD, et al. Myeloid protease-activated receptor-2 contributes to influenza A virus pathology in mice. *Front Immunol* 2021;12:791017.
[29] Abbas AA, Diamond JM, Chehoud C, et al. The perioperative lung transplant virome: torque teno viruses are elevated in donor lungs and show divergent dynamics in primary graft dysfunction. *Am J Transplant* 2017;17:1313–1324.
[30] Ylösmäki L, Fagerlund R, Kuisma I, Julkunen I, Saksela K. Nuclear translocation of Crk adaptor proteins by the influenza A virus NS1 protein. *Viruses* 2016;8:101.
[31] Dahl KN, Ribeiro AJ, Lammerding J. Nuclear shape, mechanics, and mechanotransduction. *Circ Res* 2008;102:1307–1318.
[32] Lee JJ, Park IH, Kwak MS, Rhee WJ, Kim SH, Shin JS. HMGB1 orchestrates STING-mediated senescence via TRIM30α modulation in cancer cells. *Cell Death Discov* 2021;7:28.
[33] Cheng LC, Zhang X, Abhinav K, et al. Shared and distinctive neighborhoods of emerin and lamin B receptor revealed by proximity labeling and quantitative proteomics. *J Proteome Res* 2022;21:2197–2210.
[34] Cai Z, Jitkaew S, Zhao J, et al. Plasma membrane translocation of trimerized MLKL protein is required for TNF-induced necroptosis. *Nat Cell Biol* 2014;16:55–65.
[35] Wang H, Sun L, Su L, et al. Mixed lineage kinase domain-like protein MLKL causes necrotic membrane disruption upon phosphorylation by RIP3. *Mol Cell* 2014;54:133–146.
[36] Zhuang Y, Xu HC, Shinde PV, et al. Fragile X mental retardation protein protects against tumour necrosis factor-mediated cell death and liver injury. *Gut* 2020;69:133–145.
[37] McFadden MJ, Sacco MT, Murphy KA, et al. FTO suppresses STAT3 activation and modulates proinflammatory interferon-stimulated gene expression. *J Mol Biol* 2022;434:167247.
[38] Cai J, Wang YL, Sheng XD, Zhang L, Lv X. Shufeng Jiedu capsule inhibits inflammation and apoptosis by activating A2AAR and inhibiting NF-κB to alleviate LPS-induced ALI. *J Ethnopharmacol* 2022;298:115661.
[39] Bergamaschi C, Pagoni M, Rosati M, et al. Reduced antibodies and innate cytokine changes in SARS-CoV-2 BNT162b2 mRNA vaccinated transplant patients with hematological malignancies. *Front Immunol* 2022;13:899972.
[40] Hagan RS, Torres-Castillo J, Doerschuk CM. Myeloid TBK1 signaling contributes to the immune response to influenza. *Am J Respir Cell Mol Biol* 2019;60:335–345.
[41] Cole SL, Ho LP. Contribution of innate immune cells to pathogenesis of severe influenza virus infection. *Clin Sci (Lond)* 2017;131:269–283.
[42] Tripathi S, Verma A, Kim EJ, White MR, Hartshorn KL. LL-37 modulates human neutrophil responses to influenza A virus. *J Leukoc Biol* 2014;96:931–938.
[43] Wolach O, Sellar RS, Martinod K, et al. Increased neutrophil extracellular trap formation promotes thrombosis in myeloproliferative neoplasms. *Sci Transl Med* 2018;10:eaan8292.
[44] Li H, Feng D, Cai Y, et al. Hepatocytes and neutrophils cooperatively suppress bacterial infection by differentially regulating lipocalin-2 and neutrophil extracellular traps. *Hepatology* 2018;68:1604–1620.
[45] Yang L, Tu L, Zhao P, et al. Attenuation of interferon regulatory factor 7 activity in local infectious sites of trachea and lung for preventing the development of acute lung injury caused by influenza A virus. *Immunology* 2019;157:37–51.
[46] Wu X, Bao L, Hu Z, et al. Ficolin A exacerbates severe H1N1 influenza virus infection-induced acute lung immunopathological injury via excessive complement activation. *Cell Mol Immunol* 2021;18:2278–2280.
[47] Jia X, Liu B, Bao L, et al. Delayed oseltamivir plus sirolimus treatment attenuates H1N1 virus-induced severe lung injury correlated with repressed NLRP3 inflammasome activation and inflammatory cell infiltration. *PLoS Pathog* 2018;14:e1007428.
[48] Hong AY, Lee SJ, Lee KB, Shin JW, Jeong EM, Kim IG. Double-stranded RNA enhances matrix metalloproteinase-1 and -13 expressions through TLR3-dependent activation of transglutaminase 2 in dermal fibroblasts. *Int J Mol Sci* 2022;23:2709.
[49] Huang WC, Liou CJ, Shen SC, et al. Urolithin A inactivation of TLR3/TRIF signaling to block the NF-κB/STAT1 axis reduces inflammation and enhances antioxidant defense in poly(I:C)-induced RAW264.7 cells. *Int J Mol Sci* 2022;23:4697.
[50] Wang Q, Fang P, He R, et al. O-GlcNAc transferase promotes influenza A virus-induced cytokine storm by targeting interferon regulatory factor-5. *Sci Adv* 2020;6:eaaz7086.
[51] Chattopadhyay S, Sen GC. dsRNA-activation of TLR3 and RLR signaling: gene induction-dependent and independent effects. *J Interferon Cytokine Res* 2014;34:427–436.
[52] Hur S. Double-stranded RNA sensors and modulators in innate immunity. *Annu Rev Immunol* 2019;37:349–375.
[53] Fujikura D, Miyazaki T. Programmed cell death in the pathogenesis of influenza. *Int J Mol Sci* 2018;19:2065.
[54] Atkin-Smith GK, Duan M, Chen W, Poon IKH. The induction and consequences of influenza A virus-induced cell death. *Cell Death Dis* 2018;9:1002.
[55] He S, Wang X. RIP kinases as modulators of inflammation and immunity. *Nat Immunol* 2018;19:912–922.
[56] Wallach D, Kang TB, Dillon CP, Green DR. Programmed necrosis in inflammation: toward identification of the effector molecules. *Science* 2016;352:aaf2154.
[57] Kang S, Fernandes-Alnemri T, Rogers C, et al. Caspase-8 scaffolding function and MLKL regulate NLRP3 inflammasome activation downstream of TLR3. *Nat Commun* 2015;6:7515.

How to cite this article: Li W, Huang C, Zeng Z, Li X, Xu J, Gong T, Zhang H, Zhang X, Wang P, Hu Y, Xu H, Song L. Influenza A virus infection activates TLR3-mediated necroptosis. *Sci Tradit Chin Med* 2026;4(1):40–49. doi: 10.1097/st9.0000000000000093